Fluorescence-detection size-exclusion chromatography utilizing nanobody technology for expression screening of membrane proteins

Fei Jin[1], Yao Wang[1], Mengqi Wang[1], Minxuan Sun[1], Motoyuki Hattori[1].

[1]*State Key Laboratory of Genetic Engineering, Shanghai Key Laboratory of Bioactive Small Molecules, Collaborative Innovation Center of Genetics and Development, Department of Physiology and Biophysics, School of Life Sciences, Fudan University, Shanghai 200438, China*

Correspondence should be addressed to M.H. (hattorim@fudan.edu.cn).

Abstract

Membrane proteins play numerous physiological roles and are thus of tremendous interest in pharmacology. Nevertheless, stable and homogeneous sample preparation is one of the bottlenecks in biophysical and pharmacological studies of membrane proteins because membrane proteins are typically unstable and poorly expressed. To overcome such obstacles, GFP fusion-based Fluorescence-detection Size-Exclusion Chromatography (FSEC) has been widely employed for membrane protein expression screening for over a decade. However, fused GFP itself may occasionally affect the expression and/or stability of the targeted membrane protein, leading to both false-positive and false-negative results in expression screening. Furthermore, GFP fusion technology is not well suited for some membrane proteins depending on their membrane topology. Here, we developed an FSEC assay utilizing nanobody (Nb) technology, named FSEC-Nb, in which targeted membrane proteins are fused to a small peptide tag and recombinantly expressed. The whole-cell extracts are solubilized, mixed with anti-peptide Nb fused to GFP and applied to a size-exclusion chromatography column attached to a fluorescence detector for FSEC analysis. FSEC-Nb enables one to

evaluate the expression, monodispersity and thermostability of membrane proteins without the need of purification by utilizing the benefits of the GFP fusion-based FSEC method, but does not require direct GFP fusion to targeted proteins. We applied FSEC-Nb to screen zinc-activated ion channel (ZAC) family proteins in the Cys-loop superfamily and membrane proteins from SARS-CoV-2 as examples of the practical application of FSEC-Nb. We successfully identified a ZAC ortholog with high monodispersity but moderate expression levels that could not be identified with the previously developed GFP fusion-free FSEC method. Consistent with the results of FSEC-Nb screening, the purified ZAC ortholog showed monodispersed particles by both negative staining EM and cryo-EM. Furthermore, we identified two membrane proteins from SARS-CoV-2 with high monodispersity and expression level by FSEC-Nb, which may facilitate structural and functional studies of SARS-CoV-2. Overall, our results show FSEC-Nb as a powerful tool for membrane protein expression screening that can provide further opportunity to prepare well-behaved membrane proteins for structural and functional studies.

Introduction

Biophysical and biochemical studies, especially the structural determination of membrane proteins, require stable and homogeneous sample preparations, the acquisition of which is often hindered by the poor expression and unstable nature of membrane proteins[1-3].

To overcome this issue, various methods have been developed[4-16]. In particular, following the pioneer works on the application of GFP fusion techniques for membrane protein expression screening[12-14], GFP fusion-based Fluorescence-detection Size-Exclusion Chromatography (FSEC) has been widely utilized for rapid evaluation of the expression status and thermostability of membrane proteins from both eukaryotes and prokaryotes[15,16].

In GFP fusion-based FSEC, recombinantly expressed GFP-fused proteins can be detected by a fluorescence detector following size-exclusion chromatography. The resulting fluorescence chromatography profiles allow one to rapidly analyze the expression level, monodispersity, and stability of both unpurified and purified membrane proteins at a scale on the order of nanograms. GFP fusion-based FSEC,

which is suited for the high-throughput screening of panels of orthologs, mutations and membrane proteins under different biochemical conditions, has been shown to be powerful in determining the structure of eukaryotic and prokaryotic membrane proteins by both cryo-EM and X-ray crystallography[17-25].

Nevertheless, several significant disadvantages of this method have also been recognized.

First, because GFP is a highly stable, soluble protein, its fusion sometimes causes false-positive hits by FSEC screening. In the case of such false-positive hits, GFP fusion proteins exhibit monodispersity by FSEC, but target membrane proteins may immediately aggregate or precipitate after the removal of GFP due to the instability of the target membrane protein alone[26]. Second, in addition to the issue of false positivity, GFP fusion also causes a false negativity because it sometimes negatively affects the expression level[27,28]. Finally, depending on the membrane topology of the target membrane protein, the GFP fusion technique may be difficult to apply. For instance, GFP fusion technology is not well suited for application with bacterial membrane proteins whose both N- and C-terminal ends are located at the periplasm because GFP

tends to fail to fold properly at the periplasm and thus does not show its fluorescence[29,30]. Likewise, eukaryotic Cys-loop receptors are also known to be unsuitable for either N- or C-terminal GFP fusion[31,32]. Thus, the insertion of GFP into the cytoplasmic loop is required for the application of GFP technology[31,32]. This finding indicates that the simple strategy of N- or C-terminal GFP fusion is not applicable to some eukaryotic membrane proteins; thus, the application of GFP fusion-based FSEC may need optimization of the position at which GFP is inserted.

To overcome such disadvantages, a GFP fusion-free FSEC method would be ideal, and a multivalent nitrilotriacetic acid (NTA) fluorescent probe called P3NTA was developed as a pioneer work of the GFP fusion-free FSEC method[9]. The P3NTA probe can bind the poly-histidine tag fused to a target membrane protein for detection by FSEC without the need for purification. However, since interactions of the P3NTA probe with poly-histidine-tagged proteins are relatively weak and nonspecific, endogenous proteins from host cells with multiple accessible histidine residues may seriously affect the detection of target proteins[33]. In particular, expression constructs of membrane proteins with high stability and monodispersity but relatively moderate

expression are hard to identify from FSEC screening by P3NTA due to its relatively weak and nonspecific detection ability. However, such expression constructs would now still be promising since structure determination by cryo-EM requires much less purified protein than that by X-ray crystallography[34].

To make further practical use of GFP fusion-free FSEC, we hypothesized that the application of other types of small peptide tags with high affinity and specificity would be ideal and that recent advances in nanobody (Nb) technologies for small peptides would meet such demands for GFP fusion-free FSEC.

Nb technology has been broadly utilized in laboratory research, clinical diagnosis and potential therapies[35]. Nbs, which are derived from the antigen-specific variable domain of the camelid heavy-chain antibody, have a molecular weight of 12-15 kDa and can be recombinantly expressed in bacteria with high yield.

Recently, the peptide tags ALFA and BC2 and the corresponding specific Nbs we refer to here as NbALFA and NbBC2, respectively, were developed[33,36]. The ALFA tag (SRLEEELRRRLTE), designed de novo, forms a stable, hydrophilic and electroneutral α-helix in solution with an extremely high affinity of ~26 pM for NbALFA[33,37]. The de

novo designed sequence of ALFA is absent in common model organisms, which makes its recognition by NbALFA unique[33]. The BC2 tag (PDRKAAVSHWQQ), derived from residues 16-27 of β–catenin, is unstructured in solution, and has a high affinity of ~1.4 nM for NbBC2[36].

Here, we developed a new type of FSEC utilizing Nb technology named FSEC-Nb. A membrane protein fused to the small peptide tag ALFA is recombinantly expressed in bacterial or eukaryotic cells. The whole-cell extracts are then solubilized and mixed with the NbALFA Nb, which is specific for the ALFA tag, fused to mEGFP[38] for FSEC analysis (Fig. 1).

To validate the method, we applied FSEC-Nb to the expression of bacterial and eukaryotic membrane proteins and showed that FSEC-Nb can be applied to ortholog screening and a thermostability assay.

Notably, we applied FSEC-Nb to orthologs of the zinc-activated ion channel (ZAC) family, a member of the Cys-loop receptor superfamily, which are unsuitable for either N- or C-terminal GFP fusion, and identified a ZAC ortholog from *Oryzias latipes* (OlZAC). However, we were not able to detect the expression of OlZAC by P3NTA, a

previously developed GFP fusion-free FSEC method. Consistent with the FSEC-Nb results, the negative staining EM and cryo-EM of the purified ZAC ortholog showed the monodispersity of the particles. Furthermore, we screened the expression of membrane proteins from SARS-CoV-2 by FSEC-Nb and identified two of them with a high level of expression and monodispersity, which could facilitate further structural and functional studies of SARS-CoV-2. Overall, our results showed FSEC-Nb as a powerful tool for expression screening of membrane proteins.

Results

Establishing the FSEC-Nb method

To overcome the disadvantages of the conventional FSEC method, we designed FSEC-Nb, which utilizes short peptides as fusion tags and Nbs specific to these peptides fused to monomerized EGFP proteins as a probe (Fig. 1).

We first applied our method to a prokaryotic ortholog of Zrt/Irt-like protein (ZIP) in the *E. coli* expression system. ZIPs function as metal transporters and are conserved from prokaryotes to eukaryotes, including humans[39]. Among the ZIP family, the

structure of the bacterial ZIP protein from *Bordetella bronchiseptica* (BbZIP) was determined by crystallography[39]; we chose to utilize BbZIP to establish our FSEC-Nb system because both its N- and C-terminal ends are located at the periplasm[39], which is not well suited for application of the GFP fusion-based FSEC method in bacterial expression systems.

In our experiment, BbZIP was fused to the peptide tags ALFA and BC2 at its C-terminus and recombinantly expressed in *E. coli*. The whole-cell extract was solubilized with detergents and mixed with mEGFP-fused Nbs specific for either the ALFA or BC2 tag (Fig. 2A and 2B). After removal of the pellet by ultracentrifugation, the sample was applied to a SEC column connected to a fluorescence detector (Fig. 1). When BbZIP was probed with mEGFP-tagged NbALFA, the FSEC plots presented peaks for both the mEGFP-tagged NbALFA in complex with the ALFA peptide-tagged BbZIP and free mEGFP-tagged NbALFA (Fig. 2A), but the corresponding complex peak was not observed when BbZIP was probed with mEGFP-tagged NbBC2 (Fig. 2B). These results showed that mEGFP-NbALFA specifically recognized the ALFA peptide-tagged BbZIP protein for the detection of BbZIP expression. The reason for the

failure of mEGFP-tagged NbBC2 and the BC2 tag is unknown but may have been due to the difference between tags in terms of their affinities for their Nbs (ALFA: ~26 pM, BC2: ~1.4 nM)[33,36]. Furthermore, we tested expression of the C-terminally mEGFP-tagged BbZIP by FSEC but did not detect its expression (Fig. 2C), consistent with the finding that the C-terminal end of BbZIP is located at the periplasm[39]. We also tested expression of BbZIP C-terminally fused to muGFP[40], a derivative of superfolder GFP[41], since superfolder GFP is more suitable for its folding at the periplasm[42,43]. However, we still did not detect the expression of the muGFP-tagged BbZIP by FSEC (Fig. 2C).

Overall, based on the results from BbZIP, we decided to employ the ALFA peptide tag and mEGFP-tagged NbALFA with our FSEC-Nb system for further experiments.

Thermostability assay by FSEC-Nb

We next applied the FSEC-Nb method to check membrane protein expression in mammalian cells and tested whether the FSEC-Nb system can be employed for thermostability assays of membrane proteins (Fig. 3A and 3B). We chose the human

P2X3 (hP2X3) protein, a member of the P2X receptor superfamily with known structures[44-46].

ALFA-tagged hP2X3 was transiently expressed in HEK293 cells, which were solubilized for further FSEC-Nb experiments. The FSEC profiles of ALFA-tagged hP2X3 labeled with mEGFP-fused NbALFA showed peaks for both the mEGFP-fused NbALFA in complex with the ALFA-tagged hP2X3 and free mEGFP-fused NbALFA (Fig. 3C), showing that the FSEC-Nb technique can be applied in HEK293 cells.

In the thermostability assay of hP2X3 by FSEC-Nb, solubilized samples were incubated at their respective temperatures for 10 minutes using a thermal cycler, and the precipitated materials were then removed by ultracentrifugation before labeling with mEGFP-tagged NbALFA (Fig. 3A and 3B). The FSEC-Nb profiles clearly showed a thermal shift of the main peaks from the samples incubated at temperatures near and above 55 °C (Fig. 3D), with estimates of the T_m of 56.6 °C.

We then tested the thermostabilizing effects of ATP on hP2X3 (Fig. 3E). ATP is an endogenous ligand of P2X receptors that typically increases the thermostability of P2X receptors[16]. Consistently, in the thermostability assay carried out by FSEC-Nb, ATP

showed a clear stabilizing effect, increasing the estimated T_m by 15 °C. These results showed that FSEC-Nb can be employed to assay the thermostability of membrane proteins without the need for purification steps.

Expression screening of ZAC orthologs and SARS-CoV-2 membrane proteins

As examples of the practical application of FSEC-Nb, we then applied FSEC-Nb to screen ZAC family proteins and membrane proteins from SARS-CoV-2 (Fig. 4 and 5).

ZACs belong to the Cys-loop ligand-gated ion channel (LGIC) superfamily, which also includes nicotinic acetylcholine (nACh), 5-HT_3, $GABA_A$ and glycine receptors[47,48].

In addition to Zn^{2+}, the gating of ZACs, nonselective cation channels that are widely expressed in the human body, is activated by Cu^{2+} and protons[48]. Since ZACs were the last members of the Cys-loop LGIC superfamily to be discovered[47-49], their function and structure are poorly characterized.

To facilitate structural and biophysical studies of ZAC proteins, we utilized FSEC-Nb to overcome the difficulty imposed by heterogeneous ZAC expression and purification. We chose to apply FSEC-Nb to ZACs because Cys-loop LGIC superfamily proteins

were reported to be unsuitable for either N- or C-terminal GFP fusion[31,32].

ZAC genes from *Homo sapiens* (HsZAC), *Danio rerio* (DrZAC), *Oryzias latipes* (OlZAC) and *Oreochromis niloticus* (OnZAC) were synthesized with ALFA and octa-histidine tags at the C-terminus, and recombinantly expressed in HEK293 cells. The expressed ZAC orthologs were probed by mEGFP-tagged NbALFA for detection by the FSEC-Nb method. FSEC-Nb screening of ZAC orthologs showed that the profile for OlZAC exhibited a higher and sharper peak than those for other ZAC orthologs (Fig. 4A). In contrast, we could not detect the expression of the C-terminally muGFP-tagged OlZAC by FSEC (Fig. 4B). Furthermore, we could not detect the expression of OlZAC by P3NTA-based FSEC, the previously developed GFP fusion-free FSEC method (Fig. 4C), showing the improved sensitivity of FSEC-Nb over P3NTA-based FSEC.

SARS-CoV-2 is a pathogen that causes coronavirus disease 2019 (COVID-19)[50-52]. Using FSEC-Nb, we screened the expression of a series of membrane proteins from SARS-CoV-2 (Fig. 5). We identified ORF3a and ORF7b with high monodispersity and high expression level, comparable to those of hP2X3 (Fig. 5). ORF3a is an ion channel and potential target for COVID-19 therapy[53]. A mutation on ORF7b reportedly showed

higher replicative fitness[54]. Consistent with the sharp peak from FSEC-Nb, the cryo-EM structure of ORF3a was recently reported on bioRxiv[53]. Overall, our FSEC-Nb screening results may facilitate structural and functional studies of SARS-CoV-2.

Detergent screening of OlZAC

Purification of membrane proteins requires detergents to extract the proteins from the biological membrane. The type of detergent used often affects the monodispersity and stability of a membrane protein in purification; thus, detergent screening is beneficial for establishing purification protocols for membrane proteins. Furthermore, the addition of lipids and lipid-like compounds, such as cholesteryl hemisuccinate (CHS), which was shown to be useful for the purification and crystallization of various GPCRs[55-57], could also affect the stability of membrane proteins[16]. In our assay of OlZAC thermostability by FSEC-Nb, we tested multiple types of detergents for OlZAC; among these detergents were n-dodecyl-b-D-maltoside (DDM); DDM additive with CHS at a ratio of 5:1 (w:w), referred to as DDM-CHS; lauryl maltose neopentyl glycol (LMNG); and glyco-diosgenin (GDN). The FSEC-Nb profiles of OlZAC solubilized with DDM

showed a thermal shift of the main peaks from the samples incubated at temperatures near and above 60 °C (Fig. 6A), with estimates of the Tm of 60.6 °C (Fig. 6B). Unpurified ALFA-tagged OlZAC samples solubilized with the respective detergents were heat-treated at 60 °C for 10 minutes, and FSEC-Nb was applied to both heated and unheated samples for comparison (Fig. 6C). Compared to DDM, LMNG conferred better thermostability to OlZAC, whereas DDM-CHS solubilized OlZAC similarly as with DDM (Fig. 6C). The performance of GDN was similar to that of LMNG (Fig. 6C). Based on the results of detergent screening with OlZAC by FSEC-Nb, we decided to employ either DDM or DDM-CHS for protein extraction from the membrane and either LMNG or GDN for the subsequent purification steps.

Large-scale culture and purification of OlZAC

For large-scale culture in HEK293S cells, we then generated bacmid DNA for OlZAC, which was used to transfect Sf9 insect cells to prepare BacMam virus. To optimize the expression conditions, using FSEC-Nb, we performed small-scale expression screening in HEK293S cells by testing different amounts of P2 virus, incubation times, and cell

culture temperatures at 16 hours after the addition of P2 virus (Fig. 7A and 7B) and decided to choose one set of conditions for large-scale culture (1% volume P2 virus addition, 88 hours of culture at 37 °C after the addition of virus).

OlZAC was purified as described in the Methods section. Briefly, the membrane collected from cell lysates was solubilized in DDM-CHS, and the detergent was then exchanged to LMNG in the affinity chromatography steps. During size-exclusion chromatography in SEC buffer containing LMNG, the UV absorbance plot showed a symmetric peak for OlZAC and a prior void peak (Fig. 7C). A total of 2.4 liters of HEK293 cell culture yielded approximately 0.5 mg of purified OlZAC protein. Trp-based FSEC verified the monodispersity of the pooled fractions constituting the main SEC peaks (Fig. 7D), and the purity of the pooled fractions was validated by SDS-PAGE (Fig. 7E).

Negative staining EM and cryo-EM of OlZAC

To evaluate the sample quality of OlZAC, which was identified by FSEC-Nb, we performed negative staining EM and preliminary cryo-EM of OlZAC (Fig. 8).

Pioneering structural studies of other eukaryotic pLGIC members by crystallography and cryo-EM have elucidated their fundamental architecture: a pentamer comprised of an extracellular component for ligand gating, a transmembrane component for ion permeation and an intracellular component[32,58-64]. ZACs possess low amino acid sequence identity with other pLGIC members, with the closest matches exhibiting ~20% identity with ZACs[47,48]. Accordingly, little is still known about the ZAC structure.

The OlZAC purified under the apo conditions was reconstituted into amphipol by mixing with amphipols at a mass ratio of 1:20, and the detergent was removed by Bio-Beads. We tested the reconstitution of NAPol on a small scale by Trp-FSEC, which resulted in a high and symmetric peak for the amphipol-reconstituted OlZAC (Fig. S1A). NAPol is a nonionic amphipol that is soluble across a wide pH range and compatible with multivalent cations[65,66]; thus, we chose NAPol for ZACs since both pH and the presence of divalent cations are relevant to the functional status of ZACs. On a large scale, we further reconstituted OlZAC into NAPol and separated the amphipol-reconstituted OlZAC by SEC (Fig. S1B).

The amphipol-reconstituted OlZAC was then stained by uranyl acetate and observed

under an electron microscope. The images taken by the EM-CCD camera showed monodispersed OlZAC particles (Fig. 8A). Because of the high contrast after negative staining, the particles were easily recognized from the images (Fig. 8B). The particles extracted from over one hundred images were classified into several 2D classes, which validated the stoichiometry and constitution of ZACs (Fig. 8C, 8D and 8E). Similar to other pLGIC members, ZACs form a pentamer (Fig. 8E) and is composed of extracellular, transmembrane and intracellular components (Fig. 8D).

We then performed preliminary cryo-EM single-particle analysis of OlZAC with a K3 direct detection camera (Fig. 8F and 8G), which also showed monodispersed particles.

These results showed the sample quality of OlZAC identified by FSEC-Nb, which would be suitable for structural studies.

Discussion

In this work, we developed a new type of FSEC assay, named FSEC-Nb, utilizing the ALFA peptide tag and anti-ALFA peptide Nb NbALFA. In FSEC-Nb, targeted membrane proteins are tagged by the peptide tag ALFA and recombinantly expressed in

either prokaryotic or eukaryotic cells before being probed by mEGFP-tagged NbALFA for FSEC analysis (Fig. 1). We first tested two peptide tags, ALFA and BC2, and found that the peptide tag ALFA was more suitable for the detection of BbZIP by FSEC-Nb in a bacterial expression system (Fig. 2). We then applied the FSEC-Nb method for a thermostability assay (Fig. 3). As a demonstration of the practical application of FSEC-Nb, we then applied FSEC-Nb for the screening of orthologs of ZAC, a member of the Cys-loop LGIC superfamily without a known 3D structure, as well as membrane proteins from SARS-CoV-2 (Fig. 4 and 5). We then further screened different types of detergents for the purification of OlZAC (Fig. 6). Finally, using purified OlZAC (Fig. 7), we performed negative staining EM and preliminary cryo-EM, which showed the monodispersity of the purified OlZAC sample (Fig. 8).

FSEC-Nb confers the advantage of conventional GFP fusion-based FSEC but avoids the following disadvantages of GFP fusion-based FSEC.

First, GFP fusion-based FSEC is not well suited for some membrane proteins, depending on their membrane topology[29-32]. To be noted, the membrane topology prediction from 29 organisms by TransMembrane Hidden Markov Model (TMHMM)[67]

showed ~20% of multispanning membrane proteins possess both their N- and C-terminal ends at the extracellular or periplasmic sides. Furthermore, even when applicable, GFP fusion may occasionally affect the expression and/or stability of targeted membrane proteins, potentially leading to both false-positive and false-negative results[26-28]. In our recent worst case, we screened over 60 homologs of MgtC, a virulence factor in *Salmonella enterica*[68], by GFP fusion-based FSEC with the C-terminally mGFPuv-tagged expression constructs (Table S1), because the C-terminal end of MgtC is located at the cytoplasm. We identified only two of them with high monodispersity and expression level (Fig. S2). However, both two proteins aggregated and precipitated after the removal of the GFP tag. In addition, compared to the P3-NTA method, a previously developed GFP fusion-free FSEC method utilizing poly-histidine tag, FSEC-Nb showed better performance in the screening of ZAC protein orthologs (Fig. 5). Overall, FSEC-Nb would be useful for expression screening of both types of membrane proteins to which the conventional GFP fusion-based FSEC is applicable and is not applicable.

On the other hand, representing a disadvantage of our FSEC-Nb assay over the

conventional GFP fusion FSEC method, purified GFP-fused NbALFA, which acts as a probe, needs to be prepared in each laboratory that wishes to use this method. However, the purification of mEGFP-fused NbALFA would be easy for most biochemistry and structural biology laboratories, as its *E. coli* expression level is quite high (more than 10 mg of purified protein from 1 liter of *E. coli* culture), and 1 mg of mEGFP-fused NbALFA is enough for 1,000 FSEC-Nb experiments and would thus last for a couple of years with conventional laboratory usage. Furthermore, to improve access for FSEC-Nb, we have deposited the expression vectors for mEGFP- and mCherry-fused NbALFAs as well as template vectors with the ALFA tag for expression in *E. coli* (pETNb-nALFA and pETNb-cALFA) and insect (pFBNb-cALFA) and mammalian (pBMNb-cALFA) cells to the Addgene plasmid repository (Fig. 9). We have also deposited BbZIP gene in pETNb-cALFA and hP2X3 gene in pBMNb-cALFA as positive controls for FSEC-Nb. Thus, FSEC-Nb can be easily introduced to most biochemistry and structural biology laboratories, particularly to labs those with the experience with the conventional GFP fusion-based FSEC method, which has already been widely used. Notably, all of these vectors can be used for not only a small-scale expression check by FSEC-Nb but also

large-scale protein expression.

Overall, FSEC-Nb can be used for expression screening and thermostability assays on a small scale with high sensitivity and specificity without the need for GFP fusion to target proteins. Such advantages of FSEC-Nb will enable us to explore further opportunities to prepare target proteins for structure determination as well as other biophysical and pharmacological studies.

Materials and Methods

Purification of mEGFP-tagged Nbs

With an interval of GSGSGS, the NbALFA sequence was fused in frame with an N-terminal His_8-mEGFP affinity tag and subcloned into the pET28b vector. The protein was overexpressed in *E. coli* Rosetta (DE3) cells in LB medium containing 30 μg/ml kanamycin at 37 °C by induction at an OD_{600} of ~0.5 with 0.5 mM isopropyl D-thiogalactoside (IPTG) for 16 hours at 18 °C. The *E. coli* cells were subsequently harvested by centrifugation (6,000 × g, 15 minutes) and resuspended in buffer A (50 mM Tris-HCl (pH 8.0), 150 mM NaCl) supplemented with 0.5 mM

phenylmethylsulfonyl fluoride (PMSF). All purification steps were performed at 4 °C. The *E. coli* cells were then disrupted with a microfluidizer, and debris was removed by centrifugation (70,000 × g, 60 minutes). The supernatant was loaded onto equilibrated Ni-NTA resin pre-equilibrated with buffer A and mixed for 1 hour. The column was then washed with buffer A containing 30 mM imidazole, and the protein was eluted with buffer A containing 300 mM imidazole. The imidazole was removed by dialysis in buffer B (20 mM HEPES (pH 7.0), 150 mM NaCl) overnight. Finally, the purified mEGFP-tagged NbALFA was concentrated to 1 mg/ml using an Amicon Ultra 30K filter (Merck Millipore) and stored at -80 °C before use. mEGFP-tagged NbBC was similarly expressed and purified.

FSEC-Nb in the *E. coli* expression system

In the *E. coli* expression system, BbZIP tagged with either the ALFA or BC2 peptide at its C-terminus was synthesized and subcloned into the pET28b vector and overexpressed with a protocol similar to that for the expression of mEGFP-tagged NbALFA described above. The *E. coli* cell pellets from 5 ml of LB culture were

suspended in 400 µl of buffer A and sonicated, and the cell debris was removed by centrifugation (20,000 × g, 10 minutes). The lysates were solubilized by mixing 500 µl of buffer A containing 2% (w:v) DDM and 0.5 mM PMSF for 1 hour, and were ultracentrifugaed (200,000 × g, 20 minutes). Unless noted, 1 µg of mEGFP-tagged NbALFA was added to the supernatant and incubated for 30 minutes. Considering the reported affinity values of NbALFA binding to an ALFA-tag (k_{on} ($M^{-1}s^{-1}$): 3.6(±0.1) x 10^5, k_{off} (s^{-1}): 9.4 (±0.2) x 10^{-6}, K_D 26 (±1) pM)[33], 30 minutes incubation would be enough for the saturation of the binding. After centrifugation (20,000 × g, 10 minutes), 50 µl of the sample was applied to a Superdex 200 Increase 10/300 GL column (GE Healthcare) equilibrated with buffer A containing 0.05% (w:v) DDM for the FSEC assay. GFP fusion-based FSEC was performed similarly but without the labeling step with mEGFP-tagged NbALFA. In the FSEC assay, fluorescence was detected using the RF-20Axs fluorescence detector for HPLC (Shimadzu, Japan) (for mEGFP, excitation: 480 nm, emission: 512 nm) (for muGFP, excitation: 480 nm, emission: 508 nm) (for mGFPuv, excitation: 395 nm, emission: 507 nm). FSEC-Nb experiments with mEGFP-tagged NbBC2 were performed with a similar protocol.

FSEC-Nb in the HEK293 expression system

hP2X3, ZAC orthologs and membrane proteins from SARS-CoV-2 containing ALFA and His_8 tags at their C-terminus were synthesized and subcloned into a derivative of the Bac-to-Bac system vector with the CMV promoter and WPRE motif. Using 3 μl of Lipofectamine 2000 (Thermo Fisher Scientific, US), 1 μg of each plasmid was transfected into 1 ml of HEK293S cells in adherent culture at a density of 0.5 million cells/ml in DMEM supplemented with 10% FBS. Cells were incubated in a CO_2 incubator (37 °C, 5% CO_2) for 48 hours after transfection and solubilized with 200 μl of buffer A containing 2% (w:v) DDM supplemented with 0.5 mM PMSF, 5.2 μg/ml aprotinin, 2 μg/ml leupeptin, and 1.4 μg/ml pepstatin A (all from Sigma-Aldrich) for 1 hour. After ultracentrifugation (200,000 × g, 20 minutes), 1 μg of mEGFP-tagged NbALFA or 2 μl of 0.5 μM P3NTA was added to and mixed into 100 μl of the supernatant for 30 minutes, Then, after centrifugation (20,000 × g, 10 minutes), 50 μl of the sample was applied to a Superdex 200 Increase 10/300 GL column (GE Healthcare) equilibrated with buffer A containing 0.05% (w:v) DDM for the FSEC assay. In the

FSEC assay, fluorescence was detected as described above. The P3NTA peptide was prepared and used for FSEC as previously described (excitation: 480 nm, emission: 520 nm)[9].

Thermostability assay by FSEC-Nb

ALFA peptide-tagged hP2X3 was expressed in HEK293 cells and solubilized as described above. Cells from 4 ml of culture were resuspended in 1.2 ml of buffer A (50 mM TRIS (pH 8.0), 150 mM NaCl) containing 2% DDM by the addition of either ATP at a final concentration of 1 mM (ATP-bound conditions) or 0.6 unit of apyrase (Sigma, USA) to remove endogenous ATP (apo conditions), rotated at 4 °C for 1 hour, and then ultracentrifuged (200,000 g, 10 minutes). One hundred microliters of the supernatant was dispensed into 1.5-ml Eppendorf tubes and incubated at the respective temperature for 10 minutes using either a thermal cycler or heat block bath. After ultracentrifugation (200,000 g, 10 minutes), the supernatant was mixed with 1 μg of mEGFP-tagged NbALFA and then centrifuged (20,000 g, 10 minutes). Then, 50 μl of the supernatant was applied to a Superdex 200 Increase 10/300 GL column (GE Healthcare)

equilibrated with buffer A containing 0.05% (w:v) DDM for the FSEC assay. We estimated the melting curves based on the peak heights and determined the melting temperatures by fitting the melting curves to a sigmoidal dose-response equation because the melting curves based on the peak heights were known to be consistent with the melting curves based on the peak area estimated by Gaussian fitting[16].

Detergent screening by FSEC-Nb

HEK293S cells expressing ALFA-tagged OlZAC were prepared as described above. The collected cells were solubilized in buffer A containing different types of detergents: 2% (w:v) DDM, 2% (w:v) DDM-CHS, 1% (w:v) LMNG, and 1% (w:v) GDN. FSEC-Nb and thermostability assays by FSEC-Nb were conducted as described above.

Expression and purification of OlZAC

OlZAC tagged with ALFA and His_8 was expressed in HEK293S GnTI$^-$ cells using a baculovirus-mediated gene transduction system in mammalian cells[69].

Small-scale expression screening to determine large-scale culture conditions was

performed by FSEC-Nb (Fig. 7A and 7B). FSEC-Nb was carried out with the protocol described above. A 800-ml culture of HEK293S GnTI$^-$ cells was grown to a density of 2.5×10^6 ml^{-1} and infected with 8 ml of P2 BacMam virus. After 16 hours of culture at 37 °C, 10 mM sodium butyrate was added, and the temperature was maintained at 37 °C for another 72 hours of culture. Then, the cells were harvested and washed with buffer A. All purification steps were performed at 4 °C. Cells were broken by sonication with protease inhibitors (1 mM PMSF, 5.2 μg/ml aprotinin, 2 μg/ml leupeptin, and 1.4 μg/ml pepstatin A, all from Sigma-Aldrich). Membrane fractions were collected by ultracentrifugation (200,000 × g, 60 minutes). The membrane was solubilized in buffer A containing 2% (w:v) DDM-CHS and supplemented with protease inhibitors (1 mM PMSF, 5.2 μg/ml aprotinin, 2 μg/ml leupeptin, and 1.4 μg/ml pepstatin A, all from Sigma-Aldrich) for 2 hours. The debris was removed by ultracentrifugation (200,000 × g, 60 minutes). The supernatant was loaded onto equilibrated TALON resin (Clontech) and then washed with buffer A containing 0.01% (w:v) LMNG and 10 mM imidazole. Protein was eluted with buffer A containing 300 mM imidazole. The eluted protein was loaded on a Superdex 200 10/300 GL column and subjected to SEC in buffer B

containing 0.01% (w:v) LMNG. The main peak fractions were pooled and concentrated to ~1 mg/ml using an Amicon Ultra 100K filter (Merck Millipore).

Amphipol reconstitution

All steps were performed at 4 °C. On a small scale, 10 µg of OlZAC (10 µl) was mixed with 200 µg of NAPol (Anatrace, dissolved in 2 µl of buffer B) and incubated for 16 hours. The detergent was removed by incubation with Bio-Beads SM-2 (Bio-Rad) for 4 hours, after which the beads were removed over a disposable Poly-Prep column. Twenty microliters of the eluent was diluted to 200 µl, and 50 µl of the sample was applied to a Superdex 200 10/300 GL column equilibrated with buffer A for Trp-based FSEC (excitation: 280 nm, emission: 325 nm). At a large scale, 500 µg of OlZAC (500 µl) was mixed with 10 mg of NAPol (Anatrace, dissolved in 100 µl of buffer B) and incubated for 16 hours. The detergent was removed with Bio-Beads SM-2 (Bio-Rad) for 4 hours, and the beads were subsequently removed over a disposable Poly-Prep column. The eluent was applied to a Superdex 200 10/300 GL column equilibrated with buffer B, and the main fractions consisting of the amphipol-reconstituted OlZAC were pooled and

concentrated to ~3 mg/ml using an Amicon Ultra 100K filter for electron microscopic analysis.

Negative staining and electron microscopy

Gilder 400 square mesh grids (AG400) were glow discharged in a PELCO easiGlow apparatus at a current of 25 mA for 30 seconds. Five microliters of protein solution (~20 μg/mL) was dropped onto the grid and allowed to remain on the grid for 1 minute. The residual protein solution was blotted from the grid edge with a piece of filter paper. The grid was covered with 2% uranyl acetate, blotted immediately, covered again with 2% uranyl acetate for 30 seconds and blotted again. After drying, the grid was observed under a Talos L120C microscope at 120 kV. In total, 133 micrographs were taken with a Ceta CCD camera at a nominal magnification of 92,000× at a pixel size of 1.55 Å. The micrographs were processed in RELION 3.0 for particle picking, extraction and 2D classification[70].

Cryo-EM data acquisition

A total of 2.5 µl of OlZAC in NAPol was applied to a glow-discharged holey carbon film grid (QUANTIFOIL, R1.2/1.3, 100 Holey Carbon Films, Au 300 mesh) blotted with a Vitrobot (FEI) system using a 3.0-s blotting time with 100% humidity at 9 °C and plunge-frozen in liquid ethane. Cryo-EM images were collected on a Titan Krios (FEI) electron microscope operated at an acceleration voltage of 300 kV. The specimen stage temperature was maintained at 80 K. Images were recorded with a K3 Summit direct electron detector camera (Gatan Inc.) set to super-resolution mode with a pixel size of 0.41 Å (a physical pixel size of 0.82 Å) and a defocus ranging from -1.3 µm to -2.0 µm. The dose rate was 20 e^{-} s^{-1}, and each movie was 1.76 seconds long, dose-fractioned into 40 frames, with an exposure of 1.3 e^{-} $Å^{-2}$ for each frame.

Gene synthesis

The gene fragments for mEGFP, muGFP, mCherry, ALFA and BC2 tags, NbALFA, NbBC2, BbZIP, ZAC, hP2X3, and membrane proteins from SARS-CoV-2 used for this research were synthesized by Genewiz (Suzhou, China).

Data availability

All data and materials are available from the authors upon reasonable request. The plasmids shown in Fig. 9 (mEGFP-NbALFA, mCherry-NbALFA, pETNb-nALFA, pETNb-cALFA, pFBNb-cALFA, pBMNb-cALFA) have been deposited into Addgene (http://www.addgene.org/) (Addgene IDs: 159986, 159987, 159988, 159989, 159990 and 159991). We have also deposited BbZIP gene in pETNb-cALFA and hP2X3 gene in pBMNb-cALFA as positive controls for FSEC-Nb (Addgene IDs 160498 and 160499).

Acknowledgments

We thank the staff scientists at the Center for Biological Imaging, Institute of Biophysics, and National Center for Protein Science Shanghai (Chinese Academy of Sciences) for technical support with cryo-EM data collection (project numbers: CBIapp201907006, CBIapp202001013 and 2019-NFPS-PT-004226) and Dr. Hideaki E. Kato (University of Tokyo) and Dr. Chia-Hsueh Lee (St. Jude Children's Research Hospital) for critical comments on the manuscript. This work was supported by funding from the Ministry of Science and Technology of China (2016YFA0502800) to M.H. and

from the National Natural Science Foundation of China (project 31850410466) to M.H. This work was also supported by the Shanghai Key Laboratory of Bioactive Small Molecules (ZDSYS14005) and the Innovative Research Team of High-Level Local University in Shanghai.

Author contributions

F.J. performed experiments with assistance from S.S., M.W. and Y.W. F.J. and M.H. wrote the manuscript. M.H. supervised the research. All authors discussed the manuscript.

Competing interests

The authors declare no competing interests.

References

1 Pandey, A., Shin, K., Patterson, R. E., Liu, X. Q. & Rainey, J. K. Current strategies for protein production and purification enabling membrane protein structural biology. *Biochem Cell Biol* **94**, 507-527, doi:10.1139/bcb-2015-0143 (2016).

2 Grisshammer, R. Understanding recombinant expression of membrane proteins. *Curr Opin Biotechnol* **17**, 337-340, doi:10.1016/j.copbio.2006.06.001 (2006).

3 Bill, R. M. *et al.* Overcoming barriers to membrane protein structure determination. *Nature biotechnology* **29**, 335-340, doi:10.1038/nbt.1833 (2011).

4 Alexandrov, A. I., Mileni, M., Chien, E. Y., Hanson, M. A. & Stevens, R. C. Microscale fluorescent thermal stability assay for membrane proteins. *Structure* **16**, 351-359, doi:10.1016/j.str.2008.02.004 (2008).

5 Mancusso, R., Karpowich, N. K., Czyzewski, B. K. & Wang, D. N. Simple screening method for improving membrane protein thermostability. *Methods* **55**, 324-329, doi:10.1016/j.ymeth.2011.07.008 (2011).

6 Kotov, V. *et al.* High-throughput stability screening for detergent-solubilized membrane proteins. *Sci Rep* **9**, 10379, doi:10.1038/s41598-019-46686-8 (2019).

7 Nji, E., Chatzikyriakidou, Y., Landreh, M. & Drew, D. An engineered thermal-shift screen reveals specific lipid preferences of eukaryotic and prokaryotic membrane proteins. *Nat Commun* **9**, 4253, doi:10.1038/s41467-018-06702-3 (2018).

8 Parcej, D., Guntrum, R., Schmidt, S., Hinz, A. & Tampe, R. Multicolour fluorescence-detection size-exclusion chromatography for structural genomics of membrane multiprotein complexes. *PLoS One* **8**, e67112, doi:10.1371/journal.pone.0067112 (2013).

9 Backmark, A. E. *et al.* Fluorescent probe for high-throughput screening of membrane protein expression. *Protein Sci* **22**, 1124-1132, doi:10.1002/pro.2297 (2013).

10 Morales-Perez, C. L., Noviello, C. M. & Hibbs, R. E. Manipulation of Subunit Stoichiometry in Heteromeric Membrane Proteins. *Structure* **24**, 797-805, doi:10.1016/j.str.2016.03.004 (2016).

11 Yao, H., Cai, H. & Li, D. Thermostabilization of Membrane Proteins by

Consensus Mutation: A Case Study for a Fungal Δ8-7 Sterol Isomerase. *Journal of molecular biology*, doi:10.1016/j.jmb.2020.02.015 (2020).

12 Drew, D., Lerch, M., Kunji, E., Slotboom, D. J. & de Gier, J. W. Optimization of membrane protein overexpression and purification using GFP fusions. *Nat Methods* **3**, 303-313, doi:10.1038/nmeth0406-303 (2006).

13 Drew, D. *et al.* A scalable, GFP-based pipeline for membrane protein overexpression screening and purification. *Protein science : a publication of the Protein Society* **14**, 2011-2017, doi:10.1110/ps.051466205 (2005).

14 Drew, D. E., von Heijne, G., Nordlund, P. & de Gier, J. W. Green fluorescent protein as an indicator to monitor membrane protein overexpression in Escherichia coli. *FEBS letters* **507**, 220-224, doi:10.1016/s0014-5793(01)02980-5 (2001).

15 Kawate, T. & Gouaux, E. Fluorescence-detection size-exclusion chromatography for precrystallization screening of integral membrane proteins. *Structure* **14**, 673-681, doi:10.1016/j.str.2006.01.013 (2006).

16 Hattori, M., Hibbs, R. E. & Gouaux, E. A fluorescence-detection size-exclusion chromatography-based thermostability assay for membrane protein precrystallization screening. *Structure* **20**, 1293-1299, doi:10.1016/j.str.2012.06.009 (2012).

17 Yamashita, A., Singh, S. K., Kawate, T., Jin, Y. & Gouaux, E. Crystal structure of a bacterial homologue of Na^+/Cl^--dependent neurotransmitter transporters. *Nature* **437**, 215-223, doi:10.1038/nature03978 (2005).

18 Jasti, J., Furukawa, H., Gonzales, E. B. & Gouaux, E. Structure of acid-sensing ion channel 1 at 1.9 A resolution and low pH. *Nature* **449**, 316-323, doi:10.1038/nature06163 (2007).

19 Kawate, T., Michel, J. C., Birdsong, W. T. & Gouaux, E. Crystal structure of the ATP-gated P2X4 ion channel in the closed state. *Nature* **460**, 592-598, doi:10.1038/nature08198 (2009).

20 Sobolevsky, A. I., Rosconi, M. P. & Gouaux, E. X-ray structure, symmetry and mechanism of an AMPA-subtype glutamate receptor. *Nature* **462**, 745-756, doi:10.1038/nature08624 (2009).

21 Shaffer, P. L., Goehring, A., Shankaranarayanan, A. & Gouaux, E. Structure and mechanism of a Na^+-independent amino acid transporter. *Science* **325**,

1010-1014, doi:10.1126/science.1176088 (2009).

22 Penmatsa, A., Wang, K. H. & Gouaux, E. X-ray structure of dopamine transporter elucidates antidepressant mechanism. *Nature* **503**, 85-90, doi:10.1038/nature12533 (2013).

23 Lee, C. H. *et al.* NMDA receptor structures reveal subunit arrangement and pore architecture. *Nature* **511**, 191-197, doi:10.1038/nature13548 (2014).

24 Coleman, J. A., Green, E. M. & Gouaux, E. X-ray structures and mechanism of the human serotonin transporter. *Nature* **532**, 334-339, doi:10.1038/nature17629 (2016).

25 Lu, W., Du, J., Goehring, A. & Gouaux, E. Cryo-EM structures of the triheteromeric NMDA receptor and its allosteric modulation. *Science* **355**, doi:10.1126/science.aal3729 (2017).

26 Drew, D. *et al.* GFP-based optimization scheme for the overexpression and purification of eukaryotic membrane proteins in Saccharomyces cerevisiae. *Nature protocols* **3**, 784-798, doi:10.1038/nprot.2008.44 (2008).

27 Hsieh, J. M. *et al.* Bridging the gap: a GFP-based strategy for overexpression and purification of membrane proteins with intra and extracellular C-termini. *Protein Sci* **19**, 868-880, doi:10.1002/pro.365 (2010).

28 Hammon, J., Palanivelu, D. V., Chen, J., Patel, C. & Minor, D. L., Jr. A green fluorescent protein screen for identification of well-expressed membrane proteins from a cohort of extremophilic organisms. *Protein Sci* **18**, 121-133, doi:10.1002/pro.18 (2009).

29 Feilmeier, B. J., Iseminger, G., Schroeder, D., Webber, H. & Phillips, G. J. Green fluorescent protein functions as a reporter for protein localization in Escherichia coli. *J Bacteriol* **182**, 4068-4076, doi:10.1128/jb.182.14.4068-4076.2000 (2000).

30 Daley, D. O. *et al.* Global topology analysis of the Escherichia coli inner membrane proteome. *Science* **308**, 1321-1323, doi:10.1126/science.1109730 (2005).

31 Gensler, S. *et al.* Assembly and clustering of acetylcholine receptors containing GFP-tagged epsilon or gamma subunits: selective targeting to the neuromuscular junction in vivo. *Eur J Biochem* **268**, 2209-2217, doi:10.1046/j.1432-1327.2001.02093.x (2001).

32 Hibbs, R. E. & Gouaux, E. Principles of activation and permeation in an

anion-selective Cys-loop receptor. *Nature* **474**, 54-60, doi:10.1038/nature10139 (2011).

33 Gotzke, H. *et al.* The ALFA-tag is a highly versatile tool for nanobody-based bioscience applications. *Nat Commun* **10**, 4403, doi:10.1038/s41467-019-12301-7 (2019).

34 Nogales, E. & Scheres, S. H. Cryo-EM: A Unique Tool for the Visualization of Macromolecular Complexity. *Mol Cell* **58**, 677-689, doi:10.1016/j.molcel.2015.02.019 (2015).

35 Muyldermans, S. Nanobodies: natural single-domain antibodies. *Annu Rev Biochem* **82**, 775-797, doi:10.1146/annurev-biochem-063011-092449 (2013).

36 Braun, M. B. *et al.* Peptides in headlock--a novel high-affinity and versatile peptide-binding nanobody for proteomics and microscopy. *Sci Rep* **6**, 19211, doi:10.1038/srep19211 (2016).

37 Petukhov, M. *et al.* Design of stable alpha-helices using global sequence optimization. *J Pept Sci* **15**, 359-365, doi:10.1002/psc.1122 (2009).

38 Zacharias, D. A., Violin, J. D., Newton, A. C. & Tsien, R. Y. Partitioning of lipid-modified monomeric GFPs into membrane microdomains of live cells. *Science* **296**, 913-916, doi:10.1126/science.1068539 (2002).

39 Zhang, T. *et al.* Crystal structures of a ZIP zinc transporter reveal a binuclear metal center in the transport pathway. *Sci Adv* **3**, e1700344, doi:10.1126/sciadv.1700344 (2017).

40 Scott, D. J. *et al.* A Novel Ultra-Stable, Monomeric Green Fluorescent Protein For Direct Volumetric Imaging of Whole Organs Using CLARITY. *Scientific reports* **8**, 667, doi:10.1038/s41598-017-18045-y (2018).

41 Pédelacq, J. D., Cabantous, S., Tran, T., Terwilliger, T. C. & Waldo, G. S. Engineering and characterization of a superfolder green fluorescent protein. *Nature biotechnology* **24**, 79-88, doi:10.1038/nbt1172 (2006).

42 Dinh, T. & Bernhardt, T. G. Using superfolder green fluorescent protein for periplasmic protein localization studies. *J Bacteriol* **193**, 4984-4987, doi:10.1128/jb.00315-11 (2011).

43 Dammeyer, T. & Tinnefeld, P. Engineered fluorescent proteins illuminate the bacterial periplasm. *Computational and structural biotechnology journal* **3**, e201210013, doi:10.5936/csbj.201210013 (2012).

44 Li, M. *et al.* Molecular mechanisms of human P2X3 receptor channel activation and modulation by divalent cation bound ATP. *Elife* **8**, doi:10.7554/eLife.47060 (2019).

45 Mansoor, S. E. *et al.* X-ray structures define human P2X3 receptor gating cycle and antagonist action. *Nature* **538**, 66-71, doi:10.1038/nature19367 (2016).

46 Wang, J. *et al.* Druggable negative allosteric site of P2X3 receptors. *Proc Natl Acad Sci U S A* **115**, 4939-4944, doi:10.1073/pnas.1800907115 (2018).

47 Davies, P. A., Wang, W., Hales, T. G. & Kirkness, E. F. A novel class of ligand-gated ion channel is activated by Zn^{2+}. *J Biol Chem* **278**, 712-717, doi:10.1074/jbc.M208814200 (2003).

48 Trattnig, S. M. *et al.* Copper and protons directly activate the zinc-activated channel. *Biochem Pharmacol* **103**, 109-117, doi:10.1016/j.bcp.2016.02.004 (2016).

49 Houtani, T. *et al.* Cloning and expression of ligand-gated ion-channel receptor L2 in central nervous system. *Biochem Biophys Res Commun* **335**, 277-285, doi:10.1016/j.bbrc.2005.07.079 (2005).

50 Wu, F. *et al.* A new coronavirus associated with human respiratory disease in China. *Nature* **579**, 265-269, doi:10.1038/s41586-020-2008-3 (2020).

51 Wang, C., Horby, P. W., Hayden, F. G. & Gao, G. F. A novel coronavirus outbreak of global health concern. *Lancet (London, England)* **395**, 470-473, doi:10.1016/s0140-6736(20)30185-9 (2020).

52 Zhu, N. *et al.* A Novel Coronavirus from Patients with Pneumonia in China, 2019. *The New England journal of medicine* **382**, 727-733, doi:10.1056/NEJMoa2001017 (2020).

53 Kern, D. M. *et al.* Cryo-EM structure of the SARS-CoV-2 3a ion channel in lipid nanodiscs. *bioRxiv : the preprint server for biology*, doi:10.1101/2020.06.17.156554 (2020).

54 Su, Y. C. F. *et al.* Discovery and Genomic Characterization of a 382-Nucleotide Deletion in ORF7b and ORF8 during the Early Evolution of SARS-CoV-2. *mBio* **11**, doi:10.1128/mBio.01610-20 (2020).

55 Cherezov, V. *et al.* High-resolution crystal structure of an engineered human beta2-adrenergic G protein-coupled receptor. *Science* **318**, 1258-1265, doi:10.1126/science.1150577 (2007).

56 Rasmussen, S. G. *et al.* Structure of a nanobody-stabilized active state of the beta2 adrenoceptor. *Nature* **469**, 175-180, doi:10.1038/nature09648 (2011).

57 Rosenbaum, D. M. *et al.* Structure and function of an irreversible agonist-beta2 adrenoceptor complex. *Nature* **469**, 236-240, doi:10.1038/nature09665 (2011).

58 Miller, P. S. & Aricescu, A. R. Crystal structure of a human GABAA receptor.

Nature **512**, 270-275, doi:10.1038/nature13293 (2014).

59 Huang, X., Chen, H., Michelsen, K., Schneider, S. & Shaffer, P. L. Crystal structure of human glycine receptor-alpha3 bound to antagonist strychnine. *Nature* **526**, 277-280, doi:10.1038/nature14972 (2015).

60 Du, J., Lu, W., Wu, S., Cheng, Y. & Gouaux, E. Glycine receptor mechanism elucidated by electron cryo-microscopy. *Nature* **526**, 224-229, doi:10.1038/nature14853 (2015).

61 Basak, S. *et al.* Cryo-EM structure of 5-HT3A receptor in its resting conformation. *Nat Commun* **9**, 514, doi:10.1038/s41467-018-02997-4 (2018).

62 Walsh, R. M., Jr. *et al.* Structural principles of distinct assemblies of the human alpha4beta2 nicotinic receptor. *Nature* **557**, 261-265, doi:10.1038/s41586-018-0081-7 (2018).

63 Phulera, S. *et al.* Cryo-EM structure of the benzodiazepine-sensitive alpha1beta1gamma2S tri-heteromeric GABAA receptor in complex with GABA. *Elife* **7**, doi:10.7554/eLife.39383 (2018).

64 Miyazawa, A., Fujiyoshi, Y. & Unwin, N. Structure and gating mechanism of the acetylcholine receptor pore. *Nature* **423**, 949-955, doi:10.1038/nature01748 (2003).

65 Sharma, K. S. *et al.* Non-ionic amphiphilic homopolymers: synthesis, solution properties, and biochemical validation. *Langmuir* **28**, 4625-4639, doi:10.1021/la205026r (2012).

66 Bazzacco, P. *et al.* Nonionic homopolymeric amphipols: application to

membrane protein folding, cell-free synthesis, and solution nuclear magnetic resonance. *Biochemistry* **51**, 1416-1430, doi:10.1021/bi201862v (2012).

67 Krogh, A., Larsson, B., von Heijne, G. & Sonnhammer, E. L. Predicting transmembrane protein topology with a hidden Markov model: application to complete genomes. *Journal of molecular biology* **305**, 567-580, doi:10.1006/jmbi.2000.4315 (2001).

68 Lee, J. W. & Lee, E. J. Regulation and function of the Salmonella MgtC virulence protein. *Journal of microbiology (Seoul, Korea)* **53**, 667-672, doi:10.1007/s12275-015-5283-1 (2015).

69 Goehring, A. *et al.* Screening and large-scale expression of membrane proteins in mammalian cells for structural studies. *Nat Protoc* **9**, 2574-2585, doi:10.1038/nprot.2014.173 (2014).

70 Zivanov, J. *et al.* New tools for automated high-resolution cryo-EM structure determination in RELION-3. *eLife* **7**, doi:10.7554/eLife.42166 (2018).

Figure legends

Figure 1 FSEC-Nb designation and verification

(**A**) Flow chart of FSEC-Nb for membrane protein expression and purification. (**B**) Cartoon diagram of the FSEC system for FSEC-Nb. (**C**) Cartoon of a representative FSEC trace from FSEC-Nb.

Figure 2 Establishing the FSEC-Nb method

(**A**) FSEC traces of unpurified ALFA peptide-tagged BbZIP with mEGFP-tagged NbALFA, as detected by mEGFP fluorescence. A close-up view of the main peak profiles for the complex of ALFA-tagged BbZIP and mEGFP-tagged NbALFA is also shown. (**B**) FSEC traces of unpurified BC2 peptide-tagged BbZIP with mEGFP-tagged NbBC2, as detected by mEGFP fluorescence. (**C**) FSEC traces of C-terminally mEGFP-tagged and muGFP-tagged BbZIP, as detected by mEGFP and muGFP fluorescence, respectively.

Figure 3 Thermostability assay by FSEC-Nb

(**A**) Flow chart of the thermostability assay by FSEC-Nb. (**B**) Cartoon diagram of the thermostability assay by FSEC-Nb. (**C**) FSEC-Nb traces of unpurified ALFA-tagged hP2X3, as detected by mEGFP fluorescence. (**D**) FSEC-Nb traces of unpurified ALFA-tagged hP2X3 preheated at the indicated temperatures. A close-up view of the

main peak profiles for the complex of the ALFA-tagged hP2X3 and mEGFP-tagged NbALFA is also shown. (**E**) Melting curves of hP2X3 in the presence and absence of ATP, as detected by FSEC-Nb. The fitted curves are shown as blue (apo) and green (with ATP) lines.

Figure 4 Expression screening of ZAC orthologs

(**A**) FSEC-Nb traces of unpurified ALFA peptide and His8-tagged ZAC orthologs with mEGFP-tagged NbALFA, as detected by mEGFP fluorescence. A close-up view of the main peak profiles for the complex of the ALFA-tagged ZAC and mEGFP-tagged NbALFA is also shown. The expression of ZAC orthologs from *Homo sapiens* (GI: 206725456), *Danio rerio* (528523664), *Oryzias latipes* (765127633), and *Oreochromis niloticus* (542233486) was screened by FSEC-Nb. (**B**) FSEC traces of C-terminally muGFP-tagged OlZAC, as detected by muGFP fluorescence. (**C**) FSEC traces of unpurified ALTA peptide and His8-tagged ZAC orthologs with P3NTA, as detected by fluorescein fluorescence.

Figure 5 Expression screening of membrane proteins from SARS-CoV-2

FSEC-Nb traces of unpurified ALFA peptide and His8-tagged membrane proteins from SARS-CoV-2 with mEGFP-tagged NbALFA, as detected by mEGFP fluorescence. A

close-up view of the main peak profiles is also shown. The expression of ORF3a (UniProt ID: P0DTC3), E (P0DTC4), M (P0DTC5), ORF7a (P0DTC7), and ORF7b (P0DTD8) was screened by FSEC-Nb.

Figure 6 Detergent screening for OlZAC purification

(**A**) FSEC-Nb traces of unpurified ALFA-tagged OlZAC preheated at the indicated temperatures. A close-up view of the main peak profiles is also shown. (**B**) Melting curves of OlZAC, as detected by FSEC-Nb. The fitted curve is shown as a black line. (**C**) Normalized peak heights of ALFA-tagged OlZAC preheated at 60 °C for 10 minutes solubilized with the indicated detergents. The peak heights were normalized to that from the sample solubilized with DDM at 4 °C. Error bars represent standard error of the mean (N=6).

Figure 7 Large-scale expression and purification of OlZAC

(**A**) FSEC profiles of OlZAC, as detected by FSEC-Nb for the optimization of cell culture conditions. (**B**) Time course curves of the main peak heights, as detected by FSEC-Nb. HEK293S cells were infected with P2 BacMam virus for OlZAC expression at a 1% or 2% volume. At 16 hours after virus addition, cell culture temperatures were

maintained at 37 °C or shifted to 30 °C. (**C**) Size-exclusion chromatography of OlZAC, as detected by UV absorbance. (**D**) FSEC trace of purified OlZAC, as detected by Trp fluorescence. (**E**) SDS-PAGE of the purified OlZAC after SEC.

Figure 8 Negative staining EM and cryo-EM of OlZAC

(**A, B**) Negative staining EM images of OlZAC particles. (**C-E**) Selected 2D class averages, as calculated using RELION. (**E, F**) Cryo-EM image at 1.8 μm defocused with OlZAC particles.

Figure 9 Vector maps for FSEC-Nb

(**A, B**) Maps of the expression vectors for mEGFP-tagged (**E**) and mCherry-tagged (**F**) NbALFA. (**C-F**) Maps of the expression vectors for FSEC-Nb in *E. coli* (**C, D**), insect cells (**E**), and mammalian cells (**F**).

Figure S1 Amphipol reconstitution of OlZAC

(A) FSEC trace of NaPol-reconstituted OlZAC on a small scale, as detected by Trp

fluorescence. (B) Size-exclusion chromatography of NaPol-reconstituted OlZAC, as detected by UV absorbance.

Figure S2 Expression screening of MgtC by GFP-fusion FSEC

(**A, B**) FSEC traces of C-terminally mGFPuv-tagged TpMgtC (Accession Number: WP_038038224.1) and AtMgtC (WP_043965058.1), as detected by mGFPuv fluorescence.

Table S1 MgtC orthologs for GFP fusion-based FSEC screening

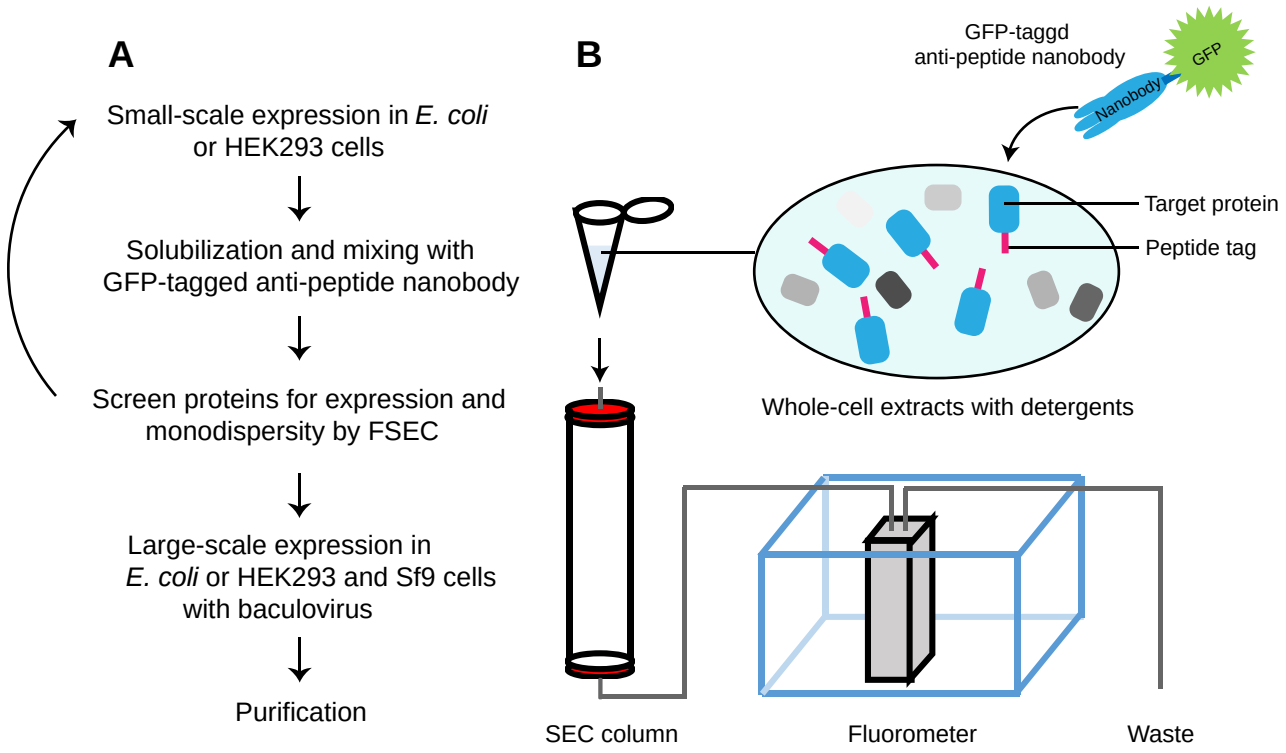

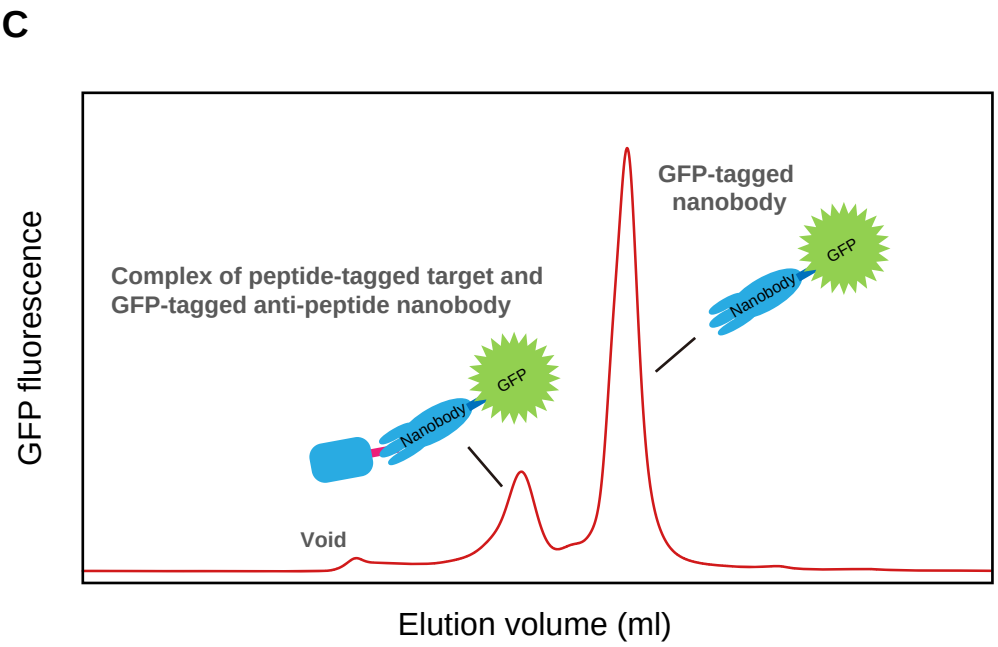

Figure 1

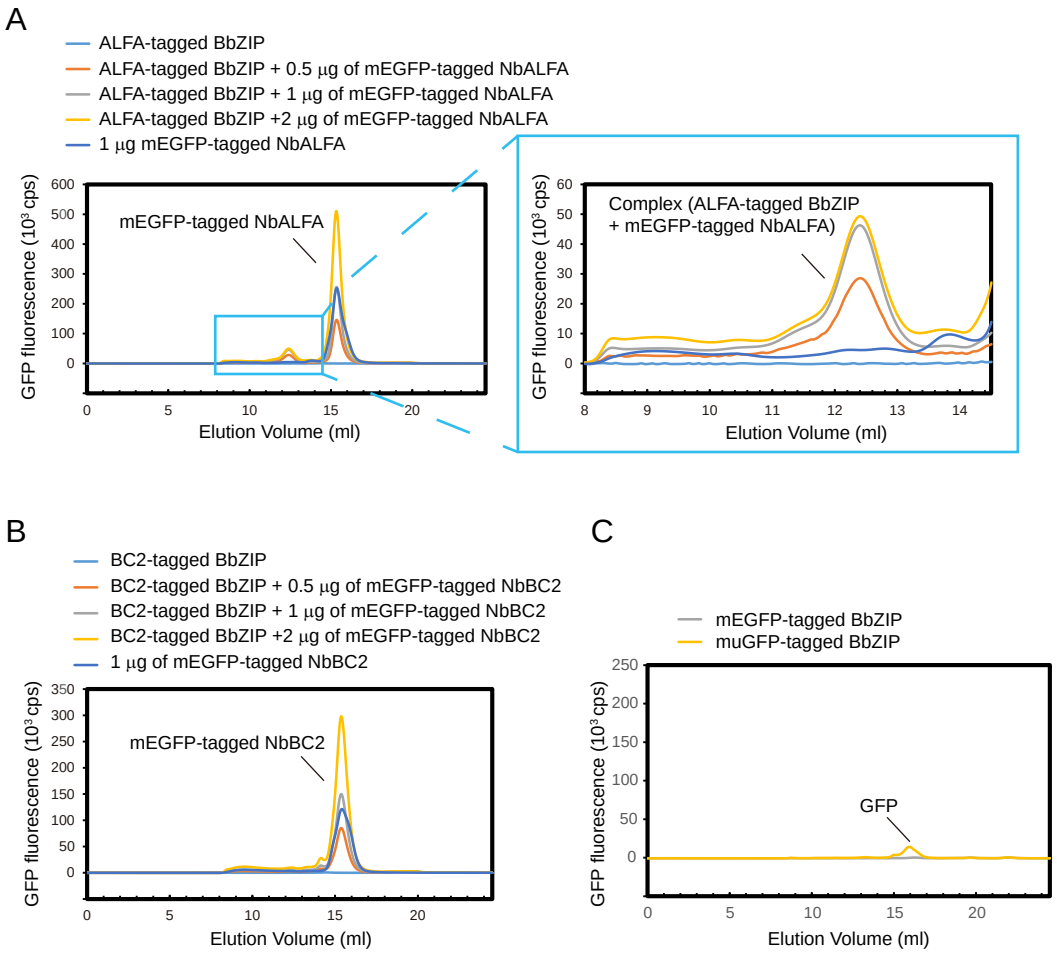

Figure 2

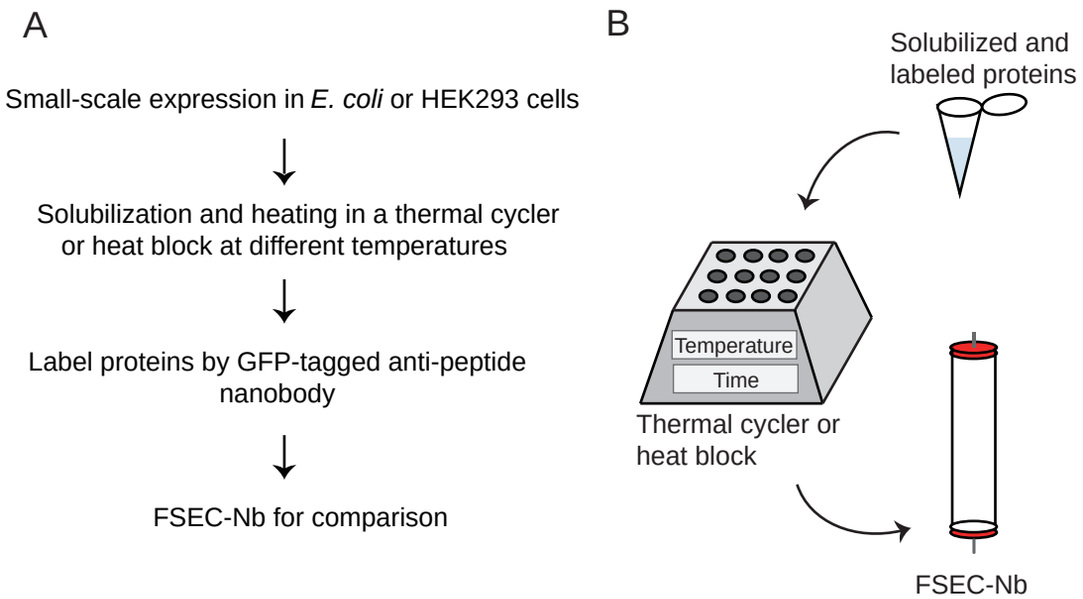

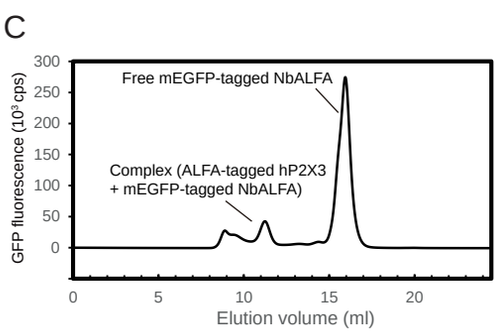

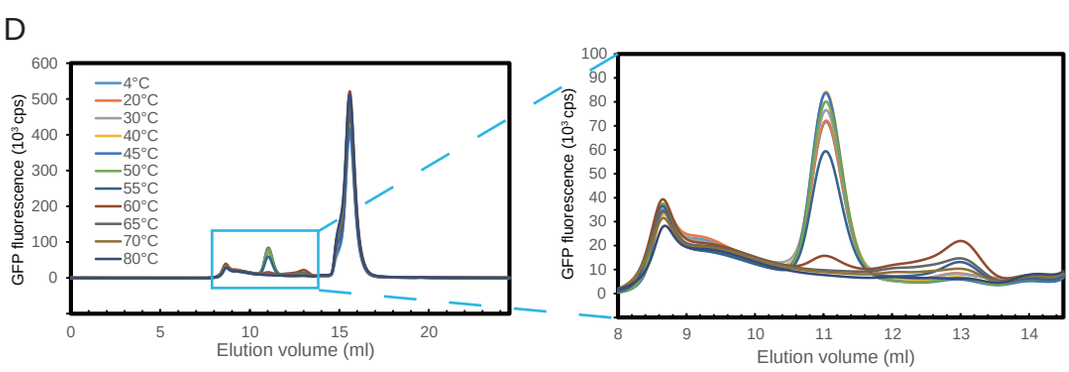

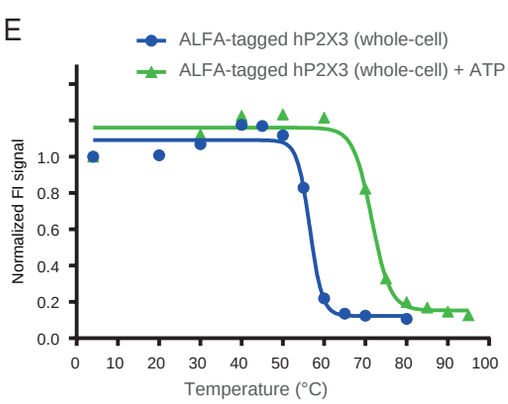

Figure 3

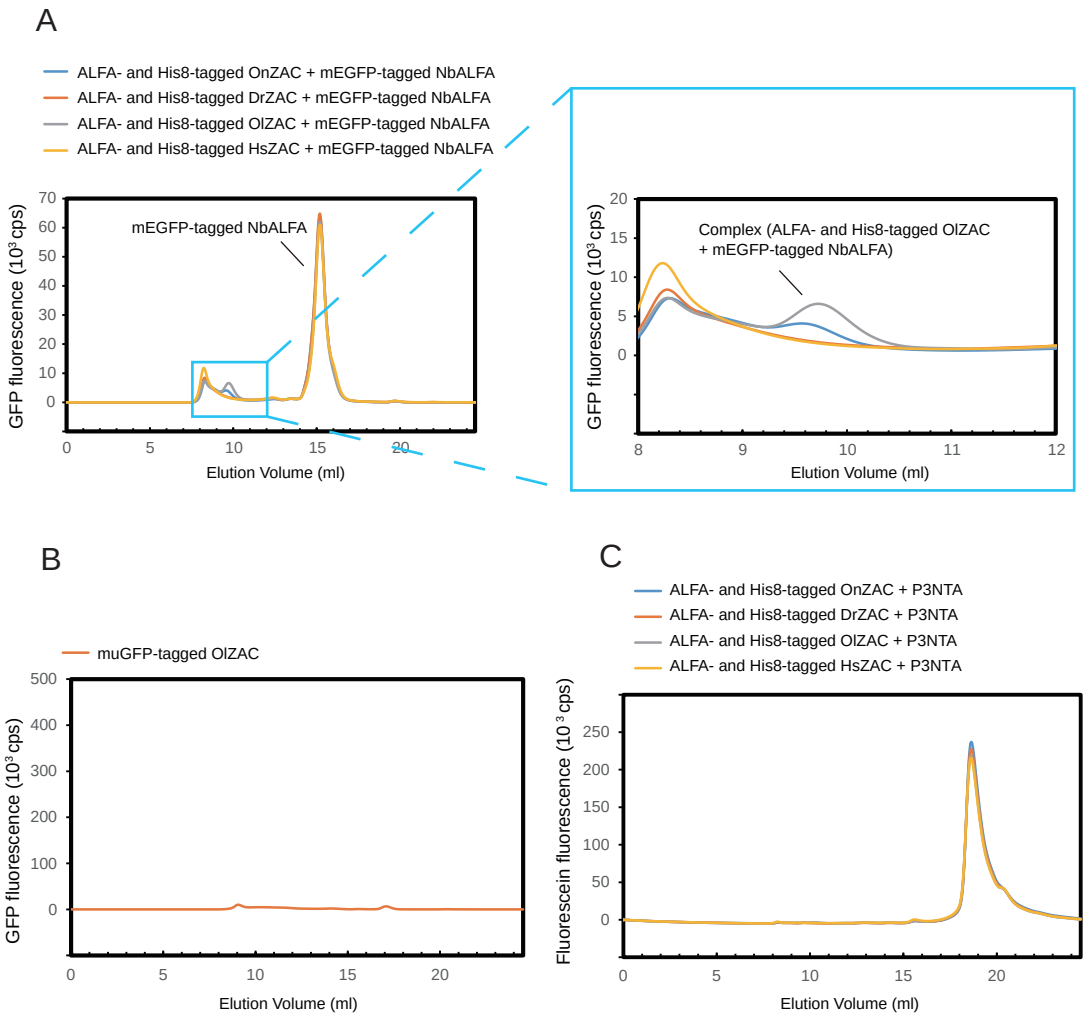

Figure 4

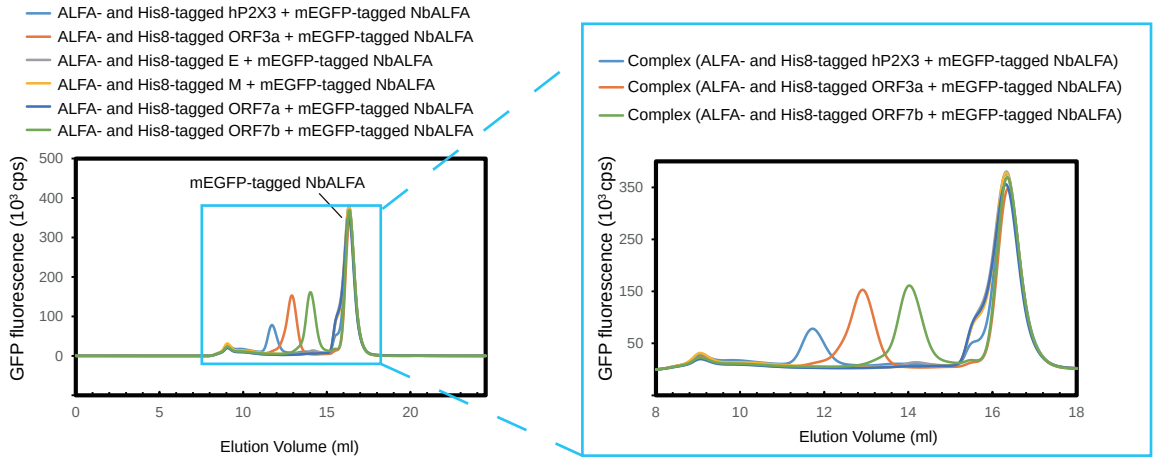

Figure 5

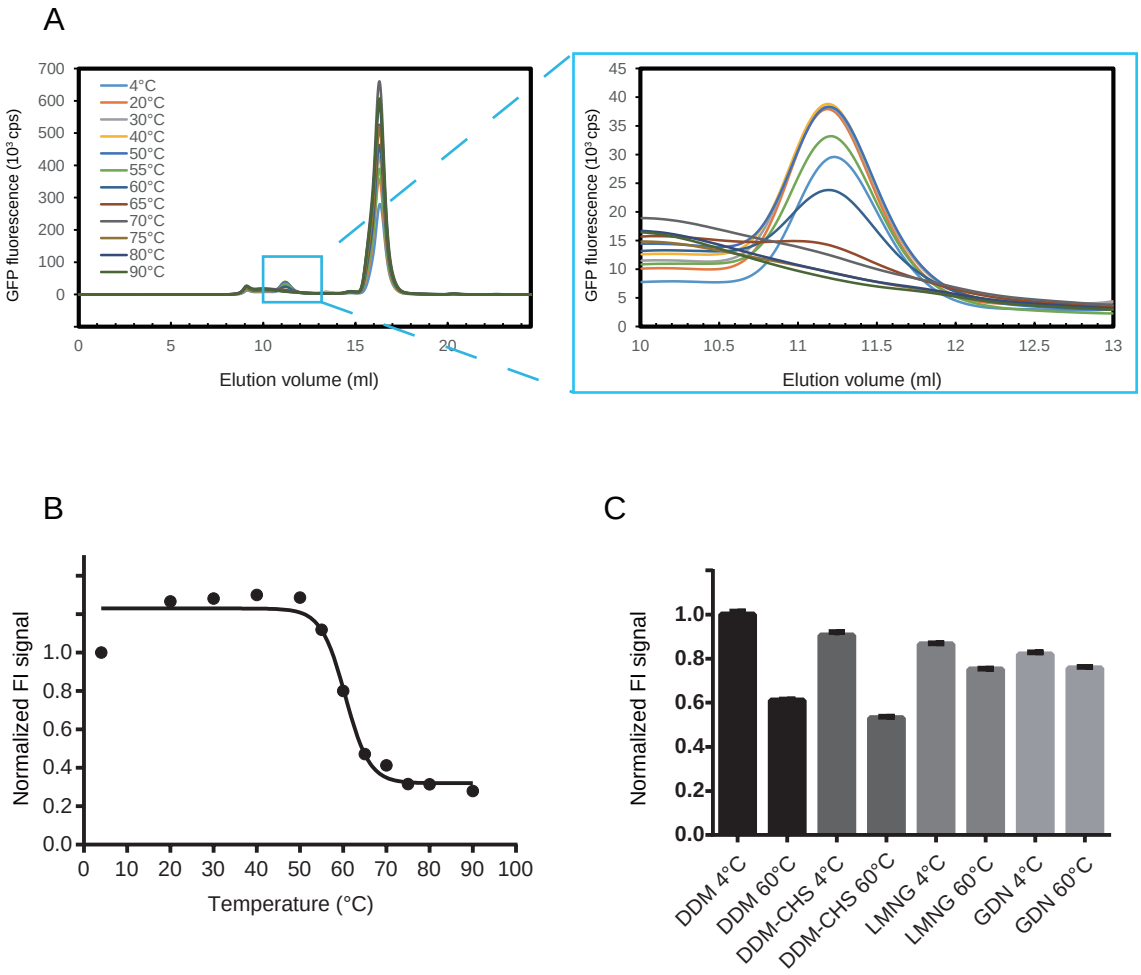

Figure 6

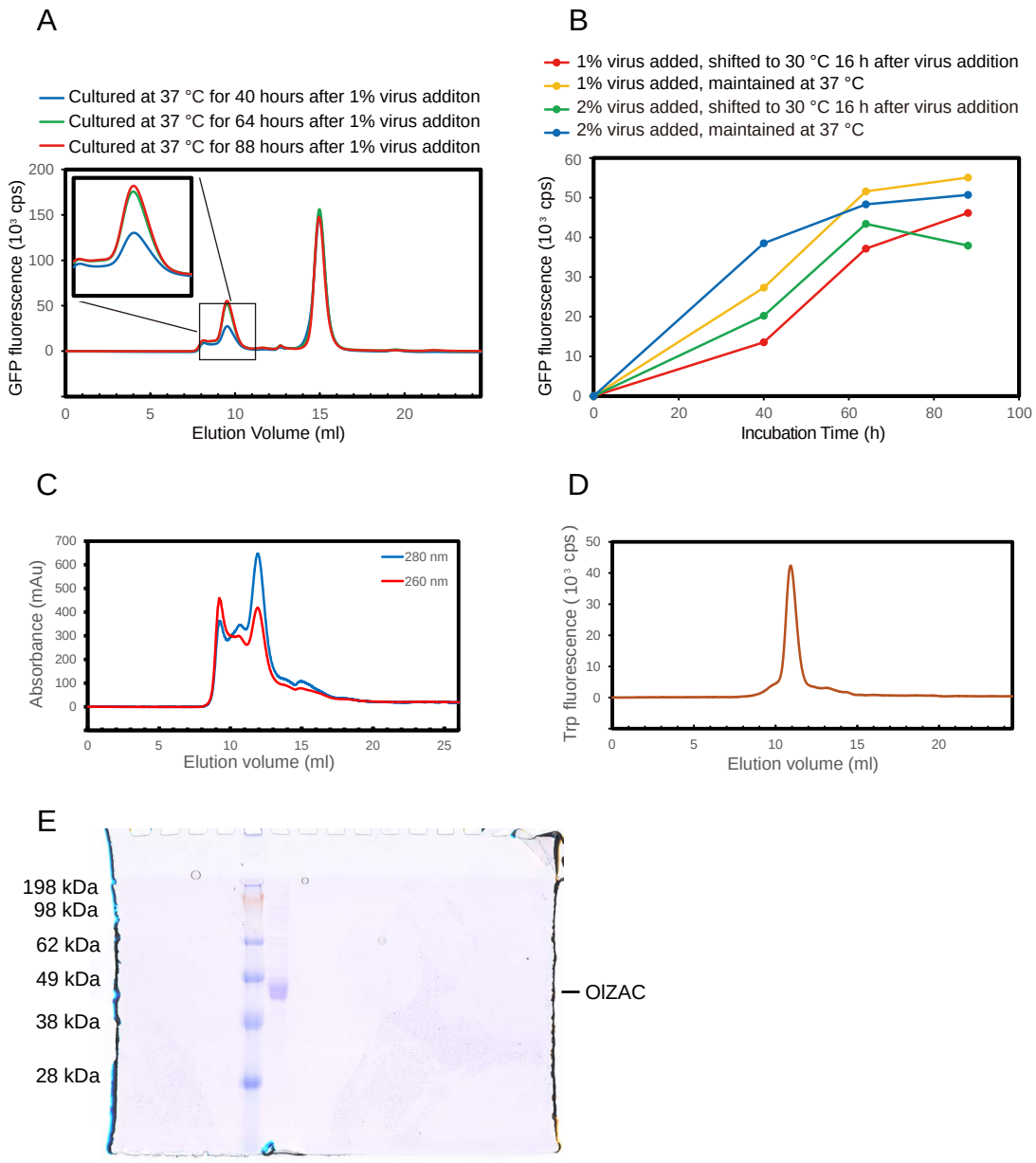

Figure 7

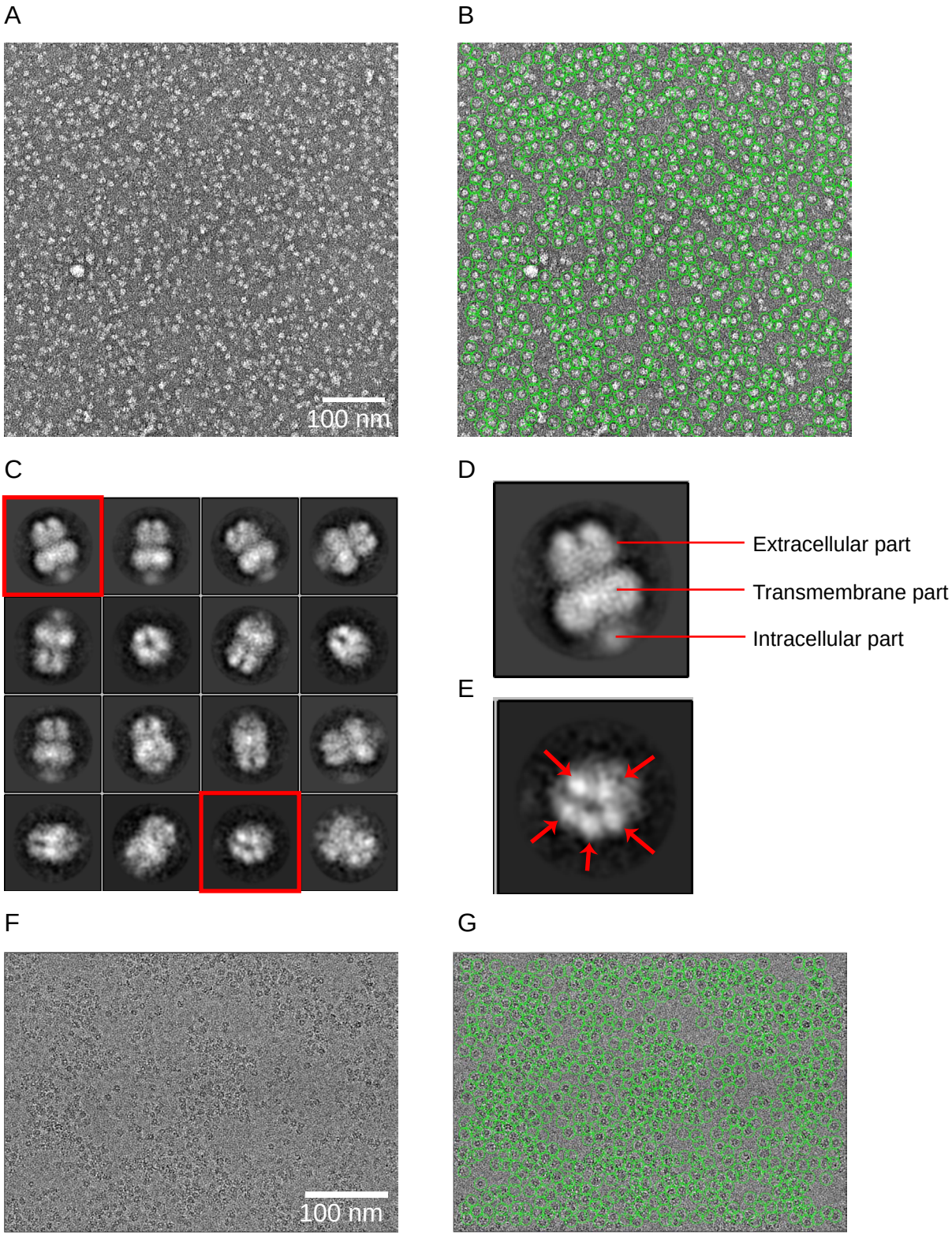

Figure 8

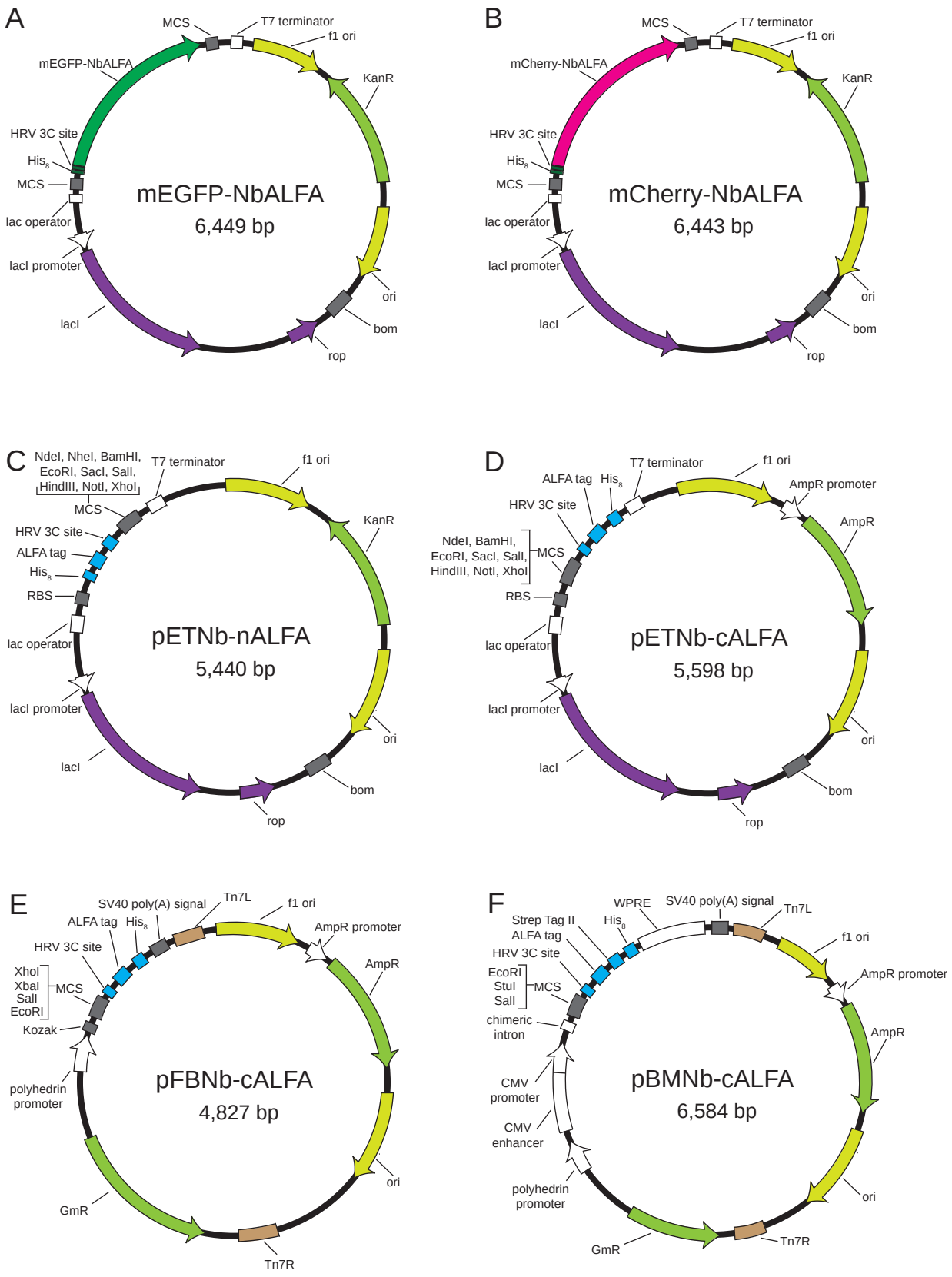

Figure 9

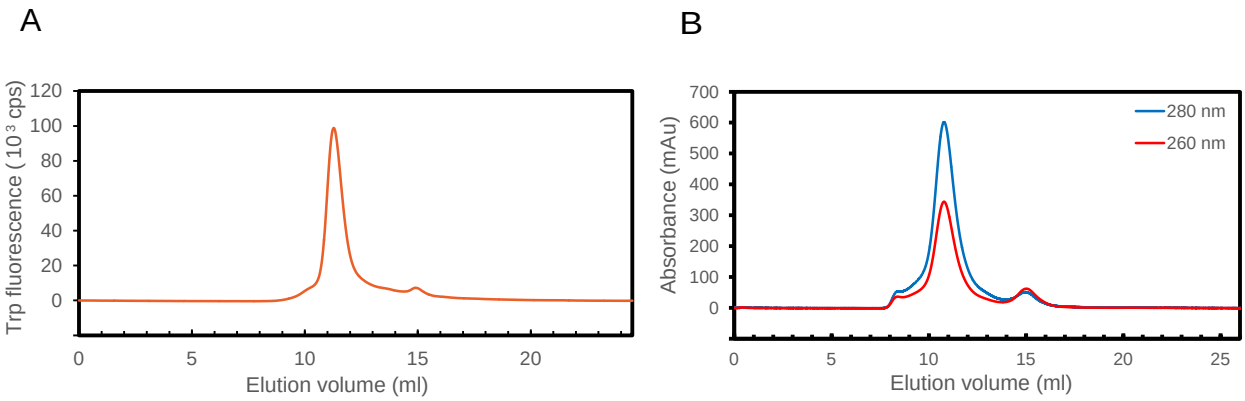

Figure S1

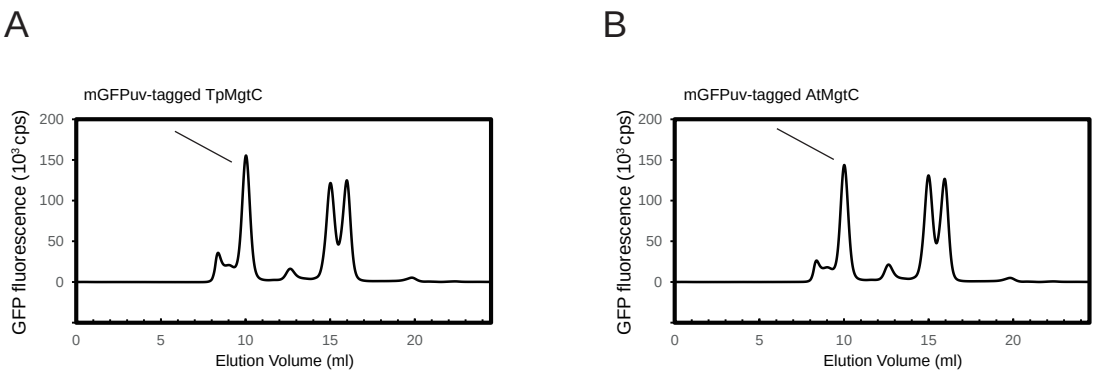

Figure S2

No	Species	Accession Number	Abbreviation
1	Halobacillus halophilus	WP_014641389.1	HhMgtC
2	Lactococcus lactis	WP_021722089.1	LlMgtC
3	Mycobacterium aromaticivorans	WP_051660484.1	MaMgtC
4	Virgibacillus halodenitrificans	WP_060678220.1	VhMgtC
5	Klebsiella oxytoca	WP_049112851.1	KoMgtC
6	Yersinia ruckeri	WP_004722955.1	YrMgtC
7	Elizabethkingia meningoseptica	WP_019051280.1	EmMgtC
8	Methylophilus sp.	WP_049639727.1	MsMgtC
9	Pedobacter agri	WP_010599226.1	PaMgtC
10	Thermobacillus composti	WP_015253117.1	TcMgtC
11	Thermobispora bispora	WP_013130974.1	TbMgtC
12	Brevibacillus brevis	WP_017246836.1	BbMgtC
13	Vibrio vulnificus	WP_045614446.1	VvMgtC
14	Clostridium acetobutylicum	WP_010966920.1	CaMgtC
15	Xanthobacter autotrophicus	WP_012113199.1	XaMgtC
16	Bacillus cereus	KYQ01271.1	BcMgtC
17	Gracilibacillus boraciitolerans	GAE93792.1	GbMgtC
18	Lactobacillus paracasei	WP_016383475.1	LpMgtC
19	Rubrobacter xylanophilus	WP_011565853.1	RxMgtC
20	Lysinibacillus boronitolerans	WP_016994404.1	LbMgtC
21	Desulfurispora thermophila	WP_018084380.1	DtMgtC
22	Thermanaerothrix daxensis	WP_054522013.1	TdMgtC
23	Thermocrinis albus	WP_012992317.1	TaMgtC
24	Sphaerobacter thermophilus	ACZ39839.1	StMgtC
25	Thermorudis peleae	WP_038038224.1	TpMgtC
26	Rubellimicrobium thermophilum	WP_040645344.1	RtMgtC
27	Quasibacillus thermotolerans	WP_039233714.1	QtMgtC
28	Thermincola ferriacetica	WP_083436703.1	TfMgtC
29	Caldicellulosiruptor naganoensis	WP_045165679.1	CnMgtC
30	Anoxybacillus thermarum	WP_043965058.1	AtMgtC
31	Desulfofundulus	WP_027355452.1	DeMgtC
32	Thermodesulfobium narugense	WP_013756617.1	TnMgtC
33	Serratia	WP_006319255.1	SeMgtC
34	Bacillus mannanilyticus	WP_025026422.1	BmMgtC
35	Alkalihalobacillus akibai	WP_035663104.1	AaMgtC
36	Hungateiclostridium thermocellum	WP_003513884.1	HtMgtC
37	Stenotrophomonas pictorum	WP_054658310.1	SpMgtC
38	Prevotella maculosa	WP_019967744.1	PmMgtC
39	Prevotella salivae	EFV04256.1	PsMgtC

40	Prevotella veroralis	WP_018911053.1	PvMgtC
41	Prevotella sp.	WP_177216065.1	PspMgtC
42	Peptococcaceae bacterium	KJS46311.1	PbMgtC
43	Sphingobacteriales bacterium	OJV97509.1	SbMgtC
44	Yersinia pestis	WP_015683614.1	YpMgtC
45	Natronincola peptidivorans	WP_090446121.1	NpMgtC
46	Myxococcus hansupus	WP_021781415.1	MhMgtC
47	Obesumbacterium proteus	WP_046459523.1	OpMgtC
48	Limihaloglobus sulfuriphilus	WP_146682549.1	LsMgtC
49	Lactobacillus kefiri	WP_054769137	LkMgtC
50	Dictyoglomus sp.	PMQ01502.1	DspMgtC
51	Bacillus sp.	WP_094032362.1	BspMgtC
52	Sphingobacterium detergens	WP_120259343.1	SdMgtC
53	Chryseobacterium culicis	WP_105683769	CcMgtC
54	Lactobacillaceae	WP_021357857.1	LaMgtC
55	Bacteroides eggerthii	WP_118363478.1	BeMgtC
56	Acidaminococcus	WP_016459447.1	AcMgtC
57	Tissierella sp. P1	WP_094904138.1	TspMgtC
58	Mucilaginibacter sp.	WP_067187481.1	MspMgtC
59	Erwinia typographi	WP_034897147.1	EtMgtC
60	Clostridium tepidiprofundi	WP_066821746.1	CtMgtC
61	Arthrobacter sp.	WP_155850019.1	AsMgtC
62	Chitinophagaceae bacterium	WP_157444983.1	CbMgtC
63	Risungbinella massiliensis	WP_044641850.1	RmMgtC
64	Deltaproteobacteria bacterium	OGR23206.1	DbMgtC
65	Carnobacterium iners	WP_085559504.1	CiMgtC
66	Lactobacillus farraginis	KRM01365.1	LfMgtC
67	Thermosyntropha lipolytica	WP_073089568.1	TlMgtC
68	Acidobacteria bacterium	PYX87356.1	AbMgtC

Table S1. MgtC orthologs for GFP fusion-based FSEC screening